KFUPM
Journal of Undergraduate Research International

Diamond Open Access 150

Article Material Science and Engineering

Enhanced Photocatalytic Performance of Ball-Milled Graphitic Carbon Nitride for Methylene Blue Degradation

Layan Mohammed Alhomidan and Muhammad Ihsan-Ul-Haq*

Cite https://doi.org/10.64589/juri/221313

Submitted: December 03, 2025 **Revised:** February 16, 2026 **Accepted:** February 25, 2026

ABSTRACT

This study examines the influence of applying a solvent-free, scalable mechanical ball-milling process on the photocatalytic performance of metal-free graphitic carbon nitride (g-C_3N_4). Structural characterization reveals that optimization of the milling time enables particle size reduction and increases the specific surface area from 5.91 to 9.16 m^2g^{-1}without affecting the inherent crystal phase. Photocatalytic analyses of Methylene Blue degradation demonstrate a pseudo-first-order reaction for the 4 h milled sample, together with a 73.73% degradation efficiency after 45 min under ultraviolet light irradiation. This is equivalent to a four-fold higher rate constant of 0.01937 min^{-1} compared with those achieved using bulk g-C_3N_4 and numerous noble-metal hybrids reported in recent literature. These findings provide useful and effective guidelines toward establishing high-performance, low-cost, metal-free photocatalysts for the rapid degradation of hazardous dyes in wastewater.

Keywords: g-C_3N_4, ball milling, photocatalysis, methylene blue, organic pollutant degradation

1. INTRODUCTION

Rapid global industrialization and textile production has led to the release of large amounts of synthetic organic dyes into aquatic ecosystems, posing a severe threat to both environmental stability and public health [1,2]. Among these pollutants, Methylene Blue (MB), which is known for its complex aromatic structure, is unresponsive to traditional biological wastewater treatment strategies [3]. MB-polluted water is associated with serious health issues, including tissue necrosis, jaundice, and respiratory distress, underscoring the need to develop more sophisticated technologies that ensure complete degradation [4,5]. Moreover, the presence of such toxins in water bodies is not regulated in many developing countries [6]. According to market report the MB market was valued at approximately $7.66 billion in 2023 and is projected to grow at an annual rate of 5.2%, reaching around $10.93 billion by 2030, thereby rendering environmental concerns increasingly significant [7]

Semiconductor-based heterogeneous photocatalysis has emerged as a key approach for environmental cleanup due to its ability to convert organic toxins into CO_2 and H_2O [8]. Although metal-oxide catalysts have been widely employed for this purpose, their wide bandgaps limit activation to the ultraviolet (UV) range, which contributes <5% of the solar spectrum [9,10]. Consequently, research has shifted toward the development of low-cost and scalable metal-free photocatalysts [11], with graphitic carbon nitride (g-C_3N_4) attracting interest as a sustainable, green photocatalyst [12,13]. However, the practical application of bulk g-C_3N_4 is hindered by its small specific surface area and high recombination rate of photogenerated electron–hole pairs [14]

To overcome these bottlenecks, recent studies have explored various modification strategies, including elemental doping [15], heterojunction construction, and morphological engineering to form two-dimensional nanosheets [16]. Despite the effectiveness of these methods, they tend to incorporate complex and expensive processes [17]. Consequently, there is an urgent need for inexpensive, simple, and chemical-free modification methods to adjust the structural and functional characteristics of g-C_3N_4 [18]. For instance, mechanical-energy-induced modifications have been demonstrated to tune the morphological features and surface electronic environments of semiconductors [19]. However, the effect of ball-milling duration on the photocatalytic activity of metal-free g-C_3N_4 has yet to be clarified [20].

The current study aims to fill this gap by investigating a low-cost, scalable, and sustainable top-down mechanical ball-milling strategy to increase catalytic activity without the requirement for chemical additives or complicated surfactants [21]. It was hypothesized that mechanical milling of g-C_3N_4 would increase its surface area and provide more abundant active sites to enhance its photocatalytic efficiency in the degradation of MB. This work aims to establish a scalable and low-cost strategy to enhance metal-free catalyst performance for sustainable environmental applications by correlating milling time, surface area, and degradation kinetics.

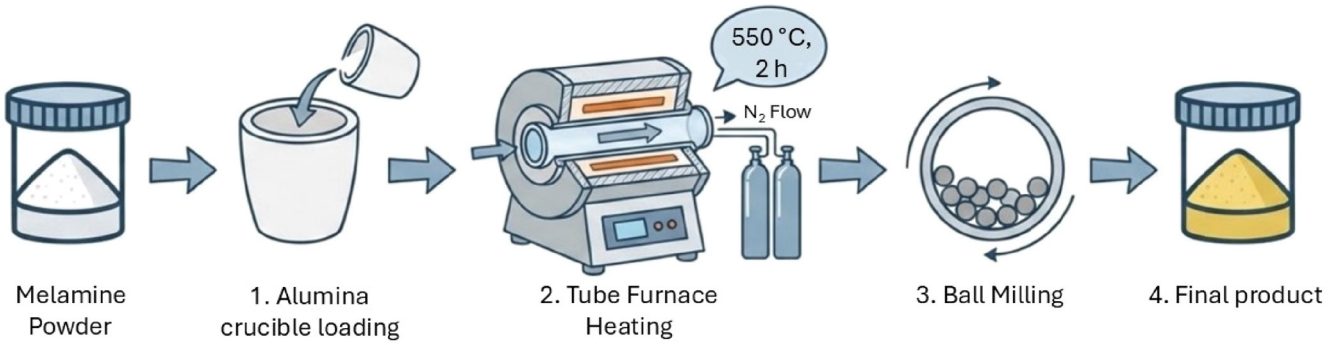

Figure 1. Schematic outline of g-C_3N_4 preparation

2. MATERIALS AND METHODS

2.1. Fabrication of the g-C_3N_4 Photocatalyst. Figure 1 outlines the experimental methodology used to prepare the target g-C_3N_4 powder. Melamine powder (5 g, 99%, Sigma-Aldrich) was placed in an alumina crucible and heated in a tube furnace under a continuous nitrogen flow (Fig. 2a). The furnace was heated to 550 °C at a heating rate of 10 °C min^{-1}, held for 2 h, and allowed to cool naturally to yield g-C_3N_4 as a yellow powder (Fig. 2b). The g-C_3N_4 surface area was modified through mechanical treatment using ball milling (MM5002 mixer mill, Retsch) at 12 Hz (720 rpm) and 23 °C, using a ball/powder mass ratio of 10:1. The samples were milled for 0 h (pristine, no milling), 2 h, or 4 h, and denoted g-C_3N_4-0h, g-C_3N_4-2h, and g-C_3N_4-4h, respectively (Fig. 2c).

2.2. Characterization . X-ray diffractometry (XRD) was used to analyze the crystallinity of the ball-milled g-C_3N_4 samples (Rigaku XRD, Cu Kα radiation source, $\lambda = 1.5406$ Å). The XRD patterns were recorded over a 2θ range of 5°–80°. Following sputter-coating with a layer of gold, the morphologies of the g-C_3N_4 samples were analyzed using scanning electron microscopy (SEM, JEOL 5800LV). The microstructural features of the g-C_3N_4 samples were examined using transmission electron microscopy (TEM, JEOL JEM-2100F) at an accelerating voltage of 200 kV. TEM samples were prepared by dispersing g-C_3N_4 powder in ethanol and drop-casting onto a holey carbon-coated copper grid followed by oven drying under air at 80 °C. The surface areas of the g-C_3N_4 samples were measured using a BELSORP MR1 surface area analyzer (Microtrac MRB). Before analysis, the samples were degassed at 120 °C for 3 h to remove any moisture or adsorbed gases. The specific surface area was determined using the Brunauer–Emmett–Teller (BET) approach to evaluate the effect of ball-milling time. The photocatalytic degradation of MB was monitored using UV–visible (UV-vis) spectroscopy (Agilent Cray-60 UV-vis spectrophotometer) between 700 and 400 nm. Spectra were recorded in absorbance mode with an average collection time of 0.075 s, data interval of 0.5 nm, and scan rate of 400 nm min^{-1}. The reported electronic bandgap for g-C_3N_4 is ~2.7 eV[22] , which enables absorption in the visible light region and is therefore critical for its photocatalytic activity in the degradation of MB. To compare the intrinsic activities of the ball-milled samples and evaluate the kinetics of MB degradation, a pseudo-first-order model was used to obtain the rate constant based on the Langmuir–Hinshelwood approach (Equation 1):[23]

$$-\ln\left(\frac{C}{C_0}\right) = kt \tag{1}$$

A plot of $\ln\left(\frac{C}{C_0}\right)$ vs. time was constructed and each dataset (0, 2, and 4 h) was fitted independently to determine the rate constant k, where the slope of each line represents the degradation rate. To evaluate degradation efficiency, the overall percentage of MB removed from the system was calculated using Equation 2:

$$Degradation\ (\%) = \left(\frac{C_0 - C_t}{C_0}\right) \times 100 \tag{2}$$

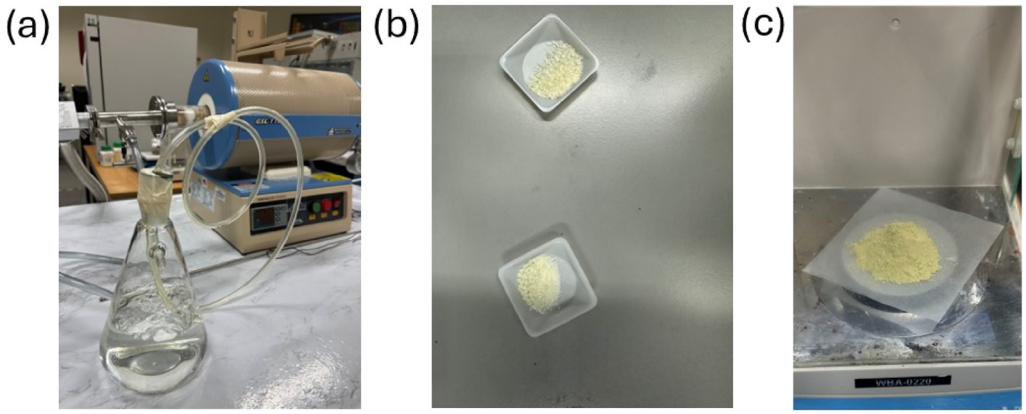

Figure 2. Photographic images of the synthesis procedure. (a) The tubular furnace used for melamine polymerization under a nitrogen atmosphere. (b) The yellow g-C_3N_4 powder obtained from the furnace. (c) The g-C_3N_4 powder after ball milling for 4 h

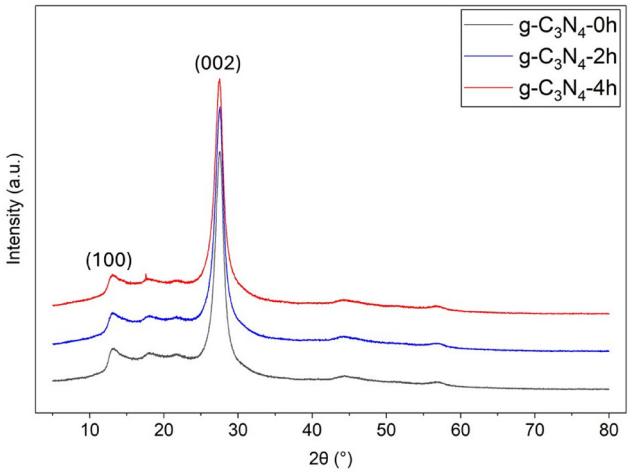

Figure 3. Stacked XRD patterns of the g-C_3N_4 samples prepared using different ball-milling durations (0, 2, and 4 h)

3. EXPERIMENTAL

To evaluate the photocatalytic efficiency of ball-milled g-C_3N_4, MB was used as a model contaminant. For each experiment, a 5 mM MB solution prepared in deionized water (50 mL) was placed in a beaker. Subsequently, the desired g-C_3N_4 photocatalyst (75 mg) was added to the solution and thoroughly dispersed by continuous magnetic stirring at 500 rpm for 30 min. The beaker was wrapped in aluminum foil to maintain dark conditions and prevent photodegradation, allowing the system to reach equilibrium and establish a baseline MB concentration for UV-vis characterization. After 30 min, the suspension was divided into two parts. One part was irradiated with a 60 W UV lamp while the other was maintained in the dark to account for any degradation originating from non-photocatalytic pathways. All experiments were repeated in triplicate for each photocatalyst variant. Aliquots were collected at fixed 15-min intervals under both irradiation conditions and analyzed using UV-vis spectrophotometry.

4. RESULTS AND DISCUSSION

4.1. XRD Analysis. The XRD patterns of the g-C_3N_4 specimens subjected to ball milling for 0, 2, and 4 h are presented in Fig. 3. All samples displayed two characteristic reflections corresponding to g-C_3N_4: a weak signal at ~13°(100), which was assigned to the in-plane structural packing of the tri-s-triazine units, and a strong peak at ~27°(002), corresponding to the interlayer stacking of conjugated aromatic layers, consistent with the standard hexagonal phase (JCPDS 87-1526)[24]. The detection of both peaks in all three samples confirms that ball milling did not alter the crystalline phase of g-C_3N_4.

However, a gradual reduction in peak intensity accompanied by slight broadening of the (002) reflection was observed with increasing milling time, suggesting decreased long-range stacking order and reduced crystallite size[25]. This is consistent with the partial exfoliation of the bulk material into thinner nanosheets, which can enhance the photocatalytic activity by increasing the number of exposed active sites and shortening the charge-transport pathways without altering the semiconducting phase of the material.

4.2. SEM Morphological Analysis . The SEM images presented in Fig. 4 clearly show a gradual decrease in particle size and reduced aggregation with increasing ball-milling time. Specifically, g-C_3N_4-0h consists of large, densely packed flakes with strong agglomeration. After 2 h of milling, the particles become noticeably smaller and the agglomerates begin to break apart, indicating partial exfoliation. The sample subjected to ball milling for 4 h exhibits the most significant decrease in particle size, with dispersed individual particles and reduced aggregation. This confirms that ball milling effectively reduced the particle size and by breaking large clusters into smaller fragments.

4.3. TEM Analysis. TEM was performed on the g-C_3N_4-4h sample to further investigate its morphology and microstructural features. The micrographs shown in Fig. 5 reveal the characteristic sheet-like morphology of g-C_3N_4, as expected after prolonged ball milling. Specifically, this nanosheet morphology indicated a greater abundance of active sites and increased light absorption capability. The absence of large agglomerates was consistent with the SEM and BET results, which revealed the largest surface area (9.16 m^2 g^{-1}) and lowest degree of aggregation among the investigated samples. These large wrinkled nanosheet clusters, which are characteristic of layered g-C_3N_4, are shown in Fig. 5a, while Fig. 5b reveals thinner, semi-transparent regions, indicating partial exfoliation. Additionally, Fig. 5c shows fragmented sheets of g-C_3N_4 with reduced stacking and increased edge exposure, whereas the high-magnification image in Fig. 5d confirms the presence of porous g-C_3N_4nanostructures.

4.4. BET Surface Area Analysis. The specific surface areas of the unmilled and ball-milled g-C_3N_4 samples were determined using a multipoint BET method. An apparent increase in surface area was observed with increasing ball-milling duration. Specifically, the unmilled powder exhibited a BET surface area of 5.91 m^2 g^{-1}, while the 2 and 4 h ball-milled samples exhibited increased areas of 8.99 and 9.16 m^2 g^{-1}, respectively, as shown in Fig. 6. These findings can be accounted for by considering that the mechanical energy imparted by prolonged ball milling continuously shears and fractures the large, bulk g-C_3N_4 flakes into thinner exfoliated nanosheets and smaller fragments, greatly increasing the external surface area available for nitrogen adsorption. Notably, an increased surface area correlates strongly with enhanced photocatalytic activity since it facilitates interfacial contact between the catalyst and the dye, thereby promoting adsorption and enhancing reaction rates. The g-C_3N_4-0h sample exhibited the lowest adsorbed volume across all relative pressures, while the g-C_3N_4-2h and g-C_3N_4-4h samples showed higher uptake, consistent with their increased surface areas.

4.5. UV-vis Analysis. To evaluate the adsorption behavior and photocatalytic activity of the synthesized photocatalysts, the degradation of MB was monitored under UV irradiation and compared with that of the MB solution stored in the dark for >75 min. UV light was used as an irradiation source to ensure

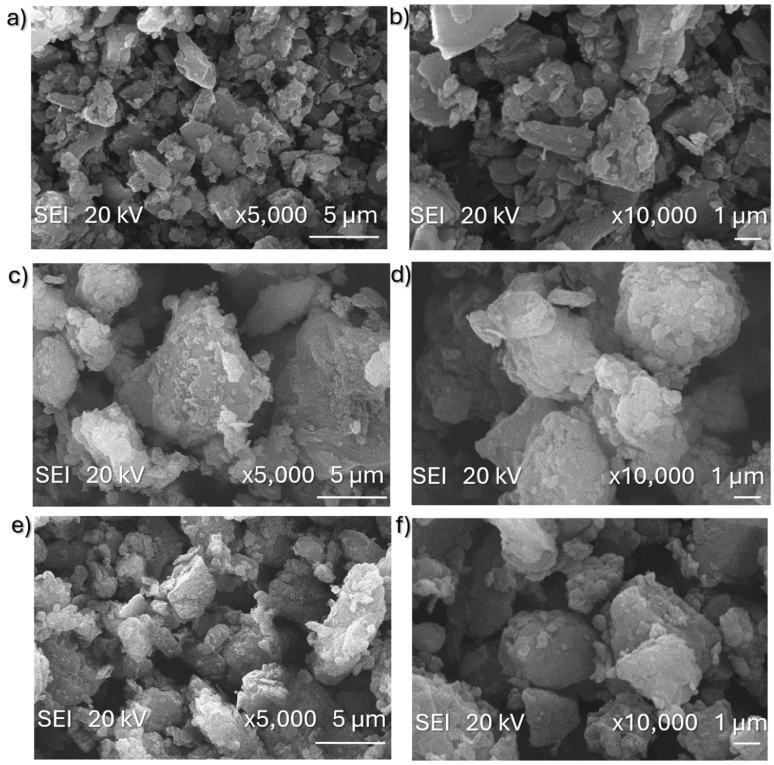

Figure 4. SEM images of the g-C_3N_4 specimens subjected to ball milling for (a, b) 0 h, (c, d) 2 h, and (e, f) 4 h. Panels (a, c, e) represent low magnification images showing the general morphology, while panels (b, d, f) are higher magnification images showing the surface texture and increased structural refinement induced by ball milling

stable and controlled photocatalytic conditions. Specifically, preliminary experiments conducted under visible solar light showed significant intermittency owing to fluctuations in light intensity, ultimately leading to solution heating and evaporation. These effects complicated data interpretation and reproducibility.

In contrast, UV irradiation provided a constant and controllable light intensity, eliminating variability associated with solar light and minimizing evaporation effects. This allowed reliable comparison of photocatalytic performance among the ball-milled g-C_3N_4 samples under identical conditions. Therefore, UV light was chosen to ensure experimental consistency, reproducibility, and fair performance evaluation.

MB exhibits a maximum characteristic absorption signal at ~664 nm; thus, the decrease in absorbance at this wavelength was tracked to assess the degree of dye degradation. Among the investigated catalysts, the samples maintained in the dark exhibited minimal reductions in MB absorbance peak intensity (Fig. 7b, 7d, and 7f), with the smallest reduction being observed for the g-C_3N_4-0h sample (Fig. 7b). The slightly enhanced reductions observed for the g-C_3N_4-2h and g-C_3N_4-4h samples (Fig. 7d

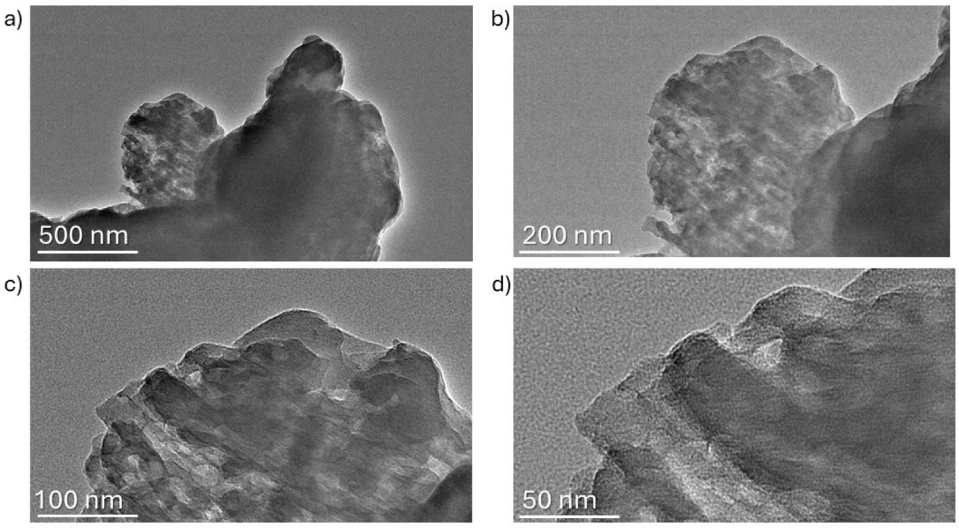

Figure 5. TEM micrographs of the g-C_3N_4-4h sample at different magnifications, with scale bars of (a) 500 nm, (b) 200 nm, (c) 100 nm, and (d) 50 nm

and 7f, respectively) were likely due to their larger surface areas. In contrast, rapid degradation was observed during UV-assisted photocatalysis, particularly for the g-C_3N_4-2h and g-C_3N_4-4h samples (Fig. 7c and 7e). The signature peak of the MB dye at ~664 nm decreased progressively with increasing UV irradiation time, confirming enhanced MB degradation via photocatalytic pathways. This reflects the role of ball milling in increasing the number of active surface sites and promoting contact between the dye and the catalyst.

A pseudo-first-order model was used to evaluate the reaction kinetics of MB degradation according to Equation 3:

$$\ln\left(\frac{C_0}{C_t}\right) = kt. \quad (3)$$

Fig. 7 shows full, unfitted kinetic plots for all samples exposed to UV irradiation for 75 min. Although all photocatalysts produced an initial linear decay region, an apparent non-linear deviation appeared after 45 min for the g-C_3N_4-4h sample. This deviation is common in photocatalytic dye degradation and is attributed to mass-transfer limitations[26]. In the early stages of the reaction, the MB concentration was high, and abundant active sites were available, facilitating adsorption kinetics and accounting for the observed linear behavior. However, after 45 min, the dye concentration decreased significantly in the g-C_3N_4-4h system (Fig. 7e) and the solution became more transparent. Beyond this point, the reaction was limited by the low dye concentration and reduced number of active sites. This behavior has been widely reported for MB, as the kinetics of the later stages become diffusion- and adsorption-controlled rather than purely photocatalytic, owing to reduced UV absorbance[27]. All samples were subjected to pseudo-first-order kinetic fitting using the Langmuir–Hinshelwood model (Fig. 8b). To ensure consistent and mathematically rigorous comparison across all photocatalysts, fitting was performed over the initial 45 min of the reaction to avoid the non-linear deviation observed for the g-C_3N_4-4h sample. The observed "bending" in the $\ln(C/C_0)$ curve violates the Langmuir–Hinshelwood model assumptions and is attributed to rapid initial removal of MB. As the dye concentration decreases significantly, the reaction transitions from being surface-controlled to being limited by mass transfer and diffusion of the remaining dye molecules to the active sites. The

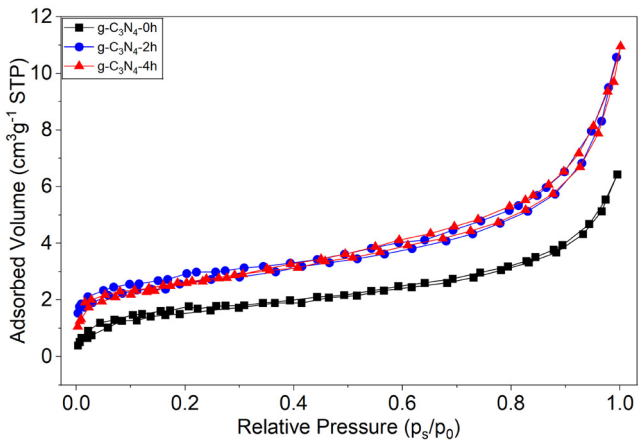

Figure 6. Nitrogen adsorption–desorption isotherms of the g-C_3N_4 samples before milling and after 2 and 4 h of milling

Table 1. *C_0 and C_t represent the maximum absorbance intensities at t = 0 and 45 min, respectively. Efficiency was calculated using Equation 2*

C_0 (arb.units)	C_{45} (arb.unis)	Efficiency (%)
0.47213	0.2276	51.80
0.62247	0.28246	54.62
0.56407	0.14819	73.73

obtained findings reveal that while the 0 h and 2 h samples maintain linear progressions for longer durations, the structural modifications and increased surface area induced by ball milling directly enhance the intrinsic early stage kinetics. Moreover, the extracted pseudo-first-order rate constants revealed distinct photocatalytic behavior among the three g-C_3N_4 samples. The g-C_3N_4-4h sample exhibited the highest initial rate constant (k = 0.01937 min^{-1}) followed by the g-C_3N_4-2h ball-milled sample (k = 0.01615 min^{-1}), and finally the g-C_3N_4-0h sample (k = 0.01584 min^{-1}). This standardized approach ensures consistency by evaluating all catalysts during their primary linear degradation phase before physical constraints, such as mass-transfer limitations and depletion of available adsorption sites, begin to dominate the reaction. By truncating the fitting window to 45 min, we account for the non-linear "bending" observed in the g-C_3N_4-4h sample's curve at later stages, which would otherwise violate the Langmuir–Hinshelwood model assumptions. This flattening after 45 min is attributed to a significant drop in MB concentration and fewer available active sites, making the reaction diffusion-controlled rather than purely photocatalytic. While the 0 h and 2 h samples maintain linear progressions for longer durations, this 45-min comparison confirms that the structural modifications and increased surface area induced by ball milling directly enhance the intrinsic early-stage kinetics.

The photocatalytic performance of the samples was subsequently evaluated by comparing the MB dye degradation efficiency after 45 min of UV light irradiation. As presented in Table 1, the absorbance intensities (C_0 and C_t) were used to determine the percentage removal, according to Equation 2.

A clear improvement trend was observed with increasing UV treatment time. Specifically, the g-C_3N_4-0h sample exhibited a baseline efficiency of 51.80%. This value increased to 54.62% for the g-C_3N_4-2h sample, while the g-C_3N_4-4h exhibited the highest photocatalytic efficiency of 73.73%. This substantial decrease in absorbance intensity indicates that ball milling for 4 h greatly increases the active surface area and promotes charge-carrier separation within the catalyst.

4.6. Comparative Study of MB Degradation Over Various g-C_3N_4 Catalysts. A comparison was subsequently performed between the g-C_3N_4-4h sample and other reported g-C_3N_4 catalysts subjected to complex chemical and noble-metal modifications. As summarized in Table 2, the 73.73% degradation efficiency for the current metal free g-C_3N_4-4h catalyst over a period of 45 min corresponded to a rate constant of 0.01937 min^{-1}. This kinetic performance is superior to that of the Ag/g-C_3N_4nanocomposite described by Nagajyothi et al. (0.01576 min^{-1}), which requires costly noble metals and a long irradiation period of 100 min[28]. Moreover, compared with the Sm_2O_3/sulfur-doped graphitic carbon nitride (CNS) heterojunction synthesized by Jourshabani et al. (0.0146

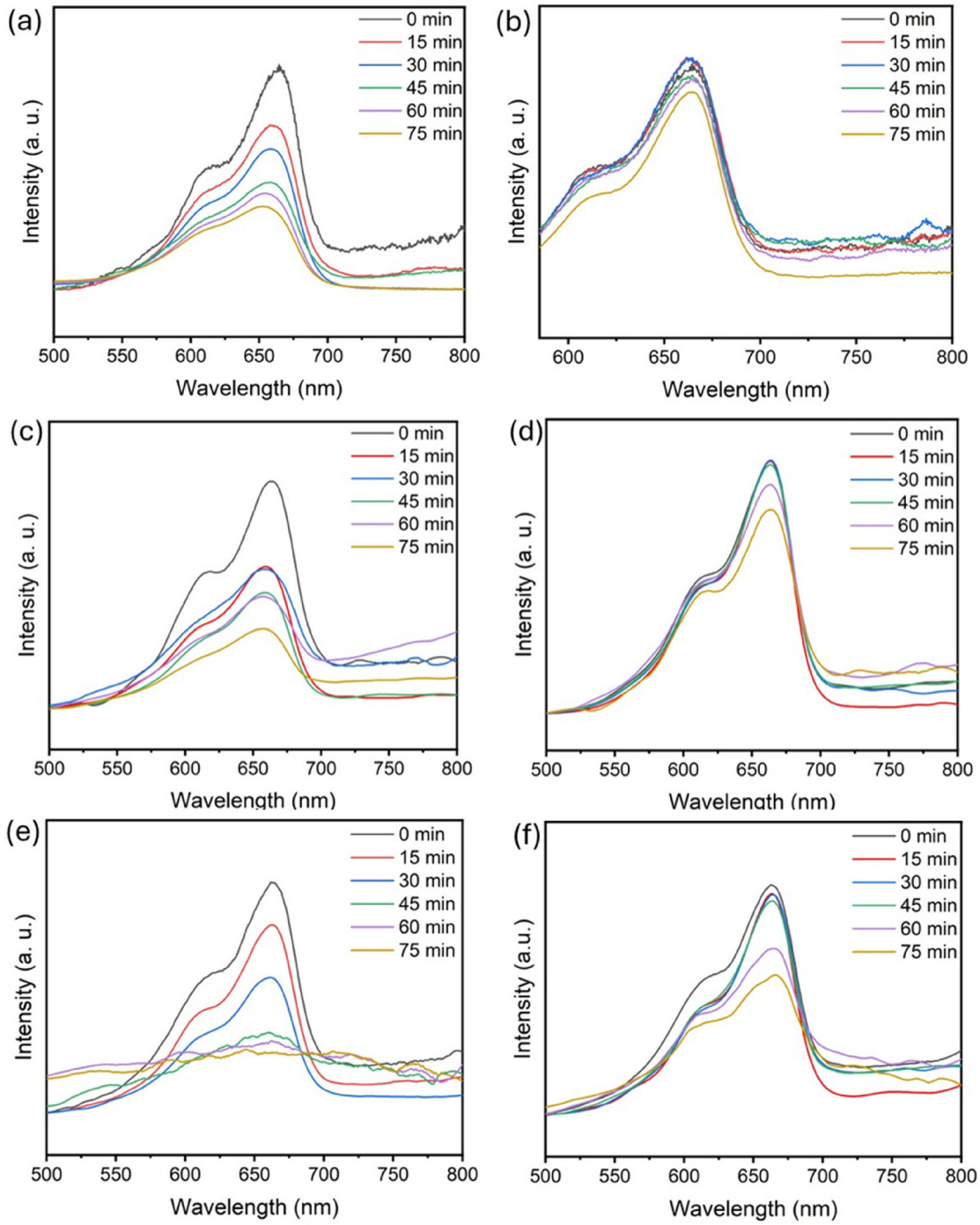

Figure 7. UV-vis plots showing the photocatalytic degradation of MB dye at different time intervals (a) g-C_3N_4-0h under UV irradiation; (b) g-C_3N_4-0h under dark conditions; (c) g-C_3N_4-2h under UV irradiation; (d) g-C_3N_4-2h under dark conditions; (e) g-C_3N_4-4h under UV irradiation; and (f) g-C_3N_4-4h under dark conditions

min^{-1})[29], the present ball milling approach was more time-efficient. The substantial performance enhancement observed for g-C_3N_4-4h can be attributed to mechanical reduction of the crystallite size and increase of the BET surface area (i.e., from 5.91 to 9.16 m^2g^{-1}), which effectively increased the active site density without the requirement for hazardous chemical precursors or costly dopants. Consequently, this work confirms that solvent-free mechanical milling represents a vigorous and potentially competitive approach to prepare photocatalysts for wastewater treatment, yielding comparable performance to more sophisticated multicomponent photocatalytic systems.

5. CONCLUSIONS

This study demonstrates that mechanical ball milling is an effective strategy for tuning the photocatalytic behavior of g-C_3N_4 without altering its intrinsic crystal phase. The 4 h milling process successfully increased the BET surface area from 5.91 to 9.16

Table 2. *Comparison of the MB photocatalytic degradation performance and pseudo-first-order rate constants (k) between the optimized ball-milled g-C_3N_4-4h sample and various modified g-C_3N_4 materials reported in the literature*

Photocatalyst type	Modification method	Time (min)	Efficiency (%)	Rate constant k (min^{-1})	Reference
Ball milled g-C_3N_4	Ball milling (4 h)	45	73.73	0.01937	This work
g-C_3N_4-S_{10}	Co-pyrolysis ($NaNO_3$)	120	70	0.01	Chang et al.[30]
Pure g-C_3N_4	Thermal	120	40	0.0042	Chang et al.[30]
CNS (S-doped)	Chemical doping	150	54	0.044	Jourshabani et al.[29]
Pristine g-C_3N_4	Thermal	100	48	0.00626	Nagajyothi et al.[28]

m^2g^{-1}, thereby increasing the active site density. Consequently, the g-C_3N_4-4h sample exhibited the highest pseudo-first-order rate constant of 0.01937 min^{-1}, significantly outperforming the g-C_3N_4-0h (0.01584 min^{-1}) and g-C_3N_4-2h (0.01615 min^{-1}) samples, achieving 73.73% MB degradation over a 45 min period. Comparison with the literature further confirmed that this simple mechanical approach rivals the kinetics of complex noble metal hybrids such as Ag/g-C_3N_4 (0.01576 min^{-1}) and Sm_2O_3/CNS (0.0146 min^{-1}). Overall, these results demonstrate a low-cost and scalable approach for maximizing the photocatalytic efficiency of metal-free photocatalysts for the removal of hazardous organic dyes from wastewater. Future efforts should focus on the incorporation of these large-surface-area nanostructures into flow-through systems to overcome mass-transfer constraints at later reaction stages.

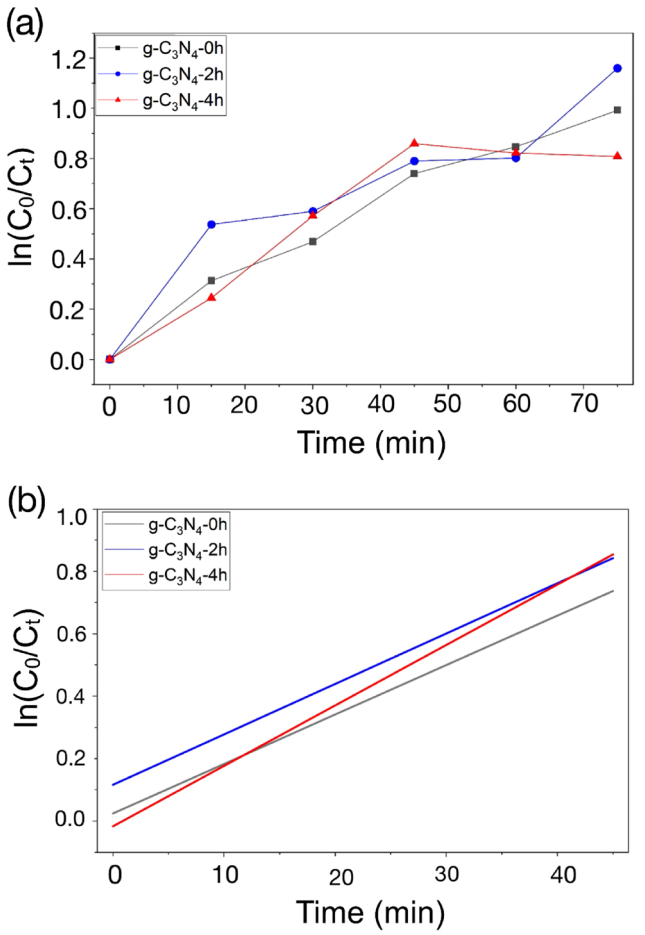

Figure 8. (a) Full kinetic plots for all samples (0, 2, and 4 h) under UV irradiation for 75 min. (b) Pseudo-first-order kinetic fitting for all samples standardized to a 45 min

AFFILIATIONS AND AUTHOR DETAILS

Undergraduate Author

Layan Mohammed Alhomidan – *Department of Materials Science and Engineering, King Fahd University of Petroleum & Minerals, Dhahran 31261, Saudi Arabia*; 0009-0004-9149-6423
Email: s202252340@kfupm.edu.sa

Corresponding Author

Muhammad Ihsan-Ul-Haq – *Research Mentor, Assistant Professor, Department of Materials Science and Engineering, Interdisciplinary Research Center for Sustainable Energy Systems, King Fahd University of Petroleum & Minerals, Dhahran 31261, Saudi Arabia*; 0000-0001-9288-0890
Email: muhammad.ihsanulhaq@kfupm.edu.sa

ACKNOWLEDGEMENTS

The authors express their sincere gratitude to the Materials Science and Engineering Department at KFUPM for providing the opportunity and resources required to conduct this study. Special appreciation is also extended to Dr. Nayef Mesnad Alsaifi, Chairman of the MSE Department, whose encouragement and belief in undergraduate research greatly supported this work. The authors acknowledge the Undergraduate Research Office for providing opportunities to conduct this project as part of the undergraduate research program. The authors acknowledge Mr. Oluwatobi Adewale Adeyeba for his assistance in the experiments. This publication is based on work supported by the King Fahd University of Petroleum and Minerals. M. I.-U.H. acknowledges the Interdisciplinary Research Center for Sustainable Energy Systems for support received under grant no. INSE 2517. The authors are grateful to the staff at the Core Research Facilities of KFUPM, who assisted with acquisition of the SEM and TEM images.

REFERENCES

(1) Al-Tohamy R, Ali SS, Li F, et al. A critical review on the treatment of dye-containing wastewater: Ecotoxicological and health concerns of textile dyes and possible remediation approaches for environmental safety. *Ecotoxicol Environ Saf.* 2022;231:113160. doi:10.1016/J.ECOENV.2021.113160

(2) xiangyu B, Chao L, Shilong H, jiping Z, Hu J. Combining advanced oxidation processes with biological processes in organic wastewater treatment: Recent developments, trends, and advances. *Desalination Water Treat*. 2025;323:101263. doi:10.1016/J.DWT.2025.101263

(3) Turhan K, Durukan I, Ozturkcan SA, Turgut Z. Decolorization of textile basic dye in aqueous solution by ozone. *Dyes and Pigments*. 2012;92(3):897-901. doi:10.1016/J.DYEPIG.2011.07.012

(4) Dutta S, Adhikary S, Bhattacharya S, et al. Contamination of textile dyes in aquatic environment: Adverse impacts on aquatic ecosystem and human health, and its management using bioremediation. *J Environ Manage*. 2024;353:120103. doi:10.1016/J.JENVMAN.2024.120103

(5) Din MI, Khalid R, Najeeb J, Hussain Z. Fundamentals and photocatalysis of methylene blue dye using various nanocatalytic assemblies- a critical review. *J Clean Prod*. 2021;298:126567. doi:10.1016/J.JCLEPRO.2021.126567

(6) Menon K, Lopis AD, Choudhari KS, Kulkarni B, Maradur S, Kulkarni SD. Scavenger-free solar photocatalytic degradation of Textile Dyes and Antibiotics using magnetically separable bi-junctional photocatalyst. *Mater Res Bull*. 2025;181:113074. doi:10.1016/J.MATERRESBULL.2024.113074

(7) Report ID 71708 (March 2024). Methylene Blue Market: Industry Analysis and Forecast (2024–2030). Published by Maximize Market Research Pvt. Ltd, Pune, India. https://www.maximizemarketresearch.com/market-report/global-methylene-blue-market/71708/#toc (accessed October 27, 2025)

(8) Iyyappan J, Gaddala B, Gnanasekaran R, Gopinath M, Yuvaraj D, Kumar V. Critical review on wastewater treatment using photo catalytic advanced oxidation process: Role of photocatalytic materials, reactor design and kinetics. *Case Studies in Chemical and Environmental Engineering*. 2024;9:100599. doi:10.1016/J.CSCEE.2023.100599

(9) Pantoja-Espinoza JC, DelaCruz-Alderete GA, Paraguay-Delgado F. Photocatalytic Degradation of Methylene Blue Dye with g-C3N4/ZnO Nanocomposite Materials Using Visible Light. *Catalysts 2025, Vol 15,*. 2025;15(9). doi:10.3390/CATAL15090851

(10) Yi S, Cui J, Li S, Zhang L, Wang D, Lin Y. Enhanced visible-light photocatalytic activity of Fe/ZnO for rhodamine B degradation and its photogenerated charge transfer properties. *Appl Surf Sci*. 2014;319(1):230-236. doi:10.1016/J.APSUSC.2014.06.151

(11) Chu S, Wang C, Feng J, Wang Y, Zou Z. Melem: A metal-free unit for photocatalytic hydrogen evolution. *Int J Hydrogen Energy*. 2014;39(25):13519-13526. doi:10.1016/J.IJHYDENE.2014.02.052

(12) Khan MA, Mutahir S, Shaheen I, Qunhui Y, Bououdina M, Humayun M. Recent advances over the doped g-C3N4 in photocatalysis: A review. *Coord Chem Rev*. 2025;522:216227. doi:10.1016/J.CCR.2024.216227

(13) Chen L, Maigbay MA, Li M, Qiu X. Synthesis and modification strategies of g-C3N4 nanosheets for photocatalytic applications. *Advanced Powder Materials*. 2024;3(1):100150. doi:10.1016/J.APMATE.2023.100150

(14) Salehi G, Bagherzadeh M, Abazari R, Hajilo M, Taherinia D. Visible Light-Driven Photocatalytic Degradation of Methylene Blue Dye Using a Highly Efficient Mg–Al LDH@g-C3N4@Ag3PO4 Nanocomposite. *ACS Omega*. 2024;9(4):4581-4593. doi:10.1021/ACSOMEGA.3C07326

(15) Mukhtar S, Szabó-Bárdos E, Őze C, et al. g-C3N4 Modified with Metal Sulfides for Visible-Light-Driven Photocatalytic Degradation of Organic Pollutants. *Molecules 2025, Vol 30,*. 2025;30(2). doi:10.3390/MOLECULES30020253

(16) Ismael M. Environmental remediation and sustainable energy generation via photocatalytic technology using rare earth metals modified g-C3N4: A review. *J Alloys Compd*. 2023;931:167469. doi:10.1016/J.JALLCOM.2022.167469

(17) Fu J, Yu J, Jiang C, Cheng B. g-C3N4-Based Heterostructured Photocatalysts. *Adv Energy Mater*. 2018;8(3):1701503. doi:10.1002/AENM.201701503;REQUESTEDJOURNAL:JOURNAL:16146840;WGROUP:STRING:PUBLICATION

(18) Wen J, Zhou L, Tang Q, Xiao X, Sun S. Photocatalytic degradation of organic pollutants by carbon quantum dots functionalized g-C3N4: A review. *Ecotoxicol Environ Saf*. 2023;262:115133. doi:10.1016/J.ECOENV.2023.115133

(19) Sakakibara N, Shizuno M, Kanazawa T, et al. Surface-Specific Modification of Graphitic Carbon Nitride by Plasma for Enhanced Durability and Selectivity of Photocatalytic CO2 Reduction with a Supramolecular Photocatalyst. *ACS Appl Mater Interfaces*. 2023;15(10):13205-13218. doi:10.1021/ACSAMI.3C00955

(20) Wu K, Chen D, Lu S, et al. Supramolecular self-assembly synthesis of noble-metal-free (C, Ce) co-doped g-C3N4 with porous structure for highly efficient photocatalytic degradation of organic pollutants. *J Hazard Mater*. 2020;382:121027. doi:10.1016/J.JHAZMAT.2019.121027

(21) Zhang X, Li X, Yu P, et al. Photocatalytic O2 activation by metal-free carbon nitride nanotube for rapid reactive species generation and organic contaminants degradation. *J Hazard Mater*. 2023;456:131715. doi:10.1016/J.JHAZMAT.2023.131715

(22) Wang X, Maeda K, Thomas A, et al. A metal-free polymeric photocatalyst for hydrogen production from water under visible light. *Nat Mater*. 2009;8(1):76-80. doi:10.1038/nmat2317

(23) Kumar KV, Porkodi K, Rocha F. Langmuir–Hinshelwood kinetics – A theoretical study. *Catal Commun*. 2008;9(1):82-84. doi:10.1016/J.CATCOM.2007.05.019

(24) Ge L. Synthesis and photocatalytic performance of novel metal-free g-C3N4 photocatalysts. *Mater Lett*. 2011;65(17-18):2652-2654. doi:10.1016/J.MATLET.2011.05.069

(25) Gao S, Liu Y, Yue X. Sustainable and low-cost SUZ-4 synthesis and its application for Cd2+ removal. *J Clean Prod*. 2021;312:127825. doi:10.1016/J.JCLEPRO.2021.127825

(26) Boiarkina I, Pedron S, Patterson DA. An experimental and modelling investigation of the effect of the flow regime on the photocatalytic degradation of methylene blue on a thin film coated ultraviolet irradiated spinning disc reactor. *Appl Catal B*. 2011;110:14-24. doi:10.1016/J.APCATB.2011.08.008

(27) Tschirch J, Dillert R, Bahnemann D. Photocatalytic degradation of methylene blue on fixed powder layers: Which limitations are to be considered? *Journal of Advanced Oxidation Technologies*. 2008;11(2):193-198. doi:10.1515/JAOTS-2008-0202

(28) Nagajyothi PC, Pandurangan M, Vattikuti SVP, Tettey CO, Sreekanth TVM, Shim J. Enhanced photocatalytic activity of Ag/g-C3N4 composite. *Sep Purif Technol*. 2017;188(1):228-237. doi:10.1016/j.seppur.2017.07.026

(29) Jourshabani M, Shariatinia Z, Badiei A. Synthesis and characterization of novel Sm2O3/S-doped g-C3N4 nanocomposites with enhanced photocatalytic activities under visible light irradiation. *Appl Surf Sci*. 2018;427(3):375-387. doi:10.1016/j.apsusc.2017.08.051

(30) Chang F, Xie Y, Li C, et al. A facile modification of g-C3N4 with enhanced photocatalytic activity for degradation of methylene blue. *Appl Surf Sci*. 2013;280(10):967-974. doi:10.1016/j.apsusc.2013.05.127